PROCEEDINGS OF SPIE

Evaluation of metal nanoparticle- and plastic resin-based x-ray contrast agents for kidney capillary imaging

Willy Kuo, Georg Schulz, Bert Müller, Vartan Kurtcuoglu

SPIE.

Evaluation of metal nanoparticle- and plastic resin-based X-ray contrast agents for kidney capillary imaging

Willy Kuo*[a,b,c], Georg Schulz[c], Bert Müller[c], Vartan Kurtcuoglu[a,b]

[a]Institute of Physiology, University of Zurich, Winterthurerstrasse 190, 8057 Zurich, Switzerland; [b]National Centre of Competence in Research, Kidney.CH, Winterthurerstrasse 190, 8057 Zurich, Switzerland; [c]Biomaterials Science Center, Department of Biomedical Engineering, University of Basel, Gewerbestrasse 14, 4123 Allschwil, Switzerland

ABSTRACT

Injection of radiopaque substances into the vasculature followed by *post mortem* high resolution X-ray µCT imaging currently remains the primary means for capillary imaging in soft tissue. Commercial contrast agents for *in vivo* applications are, however, typically small molecular compounds that can easily diffuse across the blood vessel walls, which makes them unsuitable for *ex vivo* high resolution X-ray µCT imaging. We evaluated the suitability for kidney capillary imaging of the nanoparticle-based blood pool contrast agents Aurovist 15 nm and ExiTron nano 12000, along with the vascular casting resin µAngiofil, by *post mortem* imaging of whole mouse kidneys with 4-5 µm voxel size using the laboratory source µCT system Nanotom m. Based on the results, we identified specific obstacles to reliable capillary filling in the kidney, which will aid in the development of next-generation X-ray contrast agents and protocols.

Keywords: Biological soft tissue, absorption contrast, contrast agents, organ imaging, kidney, vasculature, blood vessels

1   INTRODUCTION

Chronic kidney disease (CKD) is characterized by a decline in renal filtration function and is prevalent in 15% of the population of the United States and 25% of the population above 65 years of age.[1] In 2016, 726,331 patients were in need of a kidney transplant or dialysis, which is required below 12.5% of remaining filtration function. Capillary loss in the kidneys is a hallmark of CKD and three-dimensional (3D) imaging of the kidney vasculature with hard X-ray micro computed tomography (µCT) is employed for quantifying the extent of capillary loss and investigating its effects on hypoxia-dependent disease progression pathways.[2–4] Injection of radiopaque substances into the vasculature followed by *post mortem* high resolution X-ray µCT imaging currently remains the primary means for capillary imaging in soft tissue.[4,5] *In vivo* methods like clinical X-ray CT, magnetic resonance imaging (MRI)[6], ultrasound imaging[7], photoacoustic[8] imaging and intravital multiphoton microscopy[9,10] feature insufficient resolution or field-of-view for capillary imaging on the whole organ scale. Methods relying on staining the tissue[11,12] and phase contrast X-ray imaging of unstained tissue[13] are capable of capturing kidney morphology, but are unable to distinguish capillaries from other hollow structures, such as kidney tubuli.

Standard iodine-based angiography X-ray contrast agents are small molecules cleared from the blood via glomerular filtration in the kidney, a process in which molecules smaller than 6 nm in hydrodynamic diameter are sieved as primary urine into the renal tubules.[14] This leads to both a reduction in contrast agent concentration in the blood vessels as well as to an increase thereof in the tubules, preventing distinction of the vascular and tubular lumina and leading to a reduction in contrast-to-noise ratio. To prevent this behavior, contrast agents larger than 6 nm are required, which are available in the class of blood pool contrast agents. This class consists mainly of surface-functionalized metal nanoparticles whose main clinical application is currently magnetic resonance imaging (MRI) with gadolinium-based contrast agents.[15] Nanoparticles based on high atomic weight elements such as gold, iron and barium are commercially available as X-ray

_____

*willy.kuo@uzh.ch; phone +41 44 635 50 56; interfacegroup.ch

contrast agents for preclinical imaging. These have been used mainly for low resolution *in vivo* imaging studies,[16–19] but high resolution *ex vivo* imaging is required to capture capillaries. This off-label application creates a different set of requirements. Most importantly, all capillaries need to be completely filled with contrast agent in a reliable and reproducible fashion, in order to judge whether tissue regions without blood vessels represent genuine capillary rarefaction or simply contrast agent filling artifacts. In this study, the reliability of two blood-pool contrast agents when filling the renal capillary network was investigated: Aurovist 15 nm, a gold-nanoparticle-based blood pool contrast agent, and ExiTron nano 12000, an alkaline earth metal-nanoparticle-based blood pool contrast agent. The performance of these agents was compared to that of μAngiofil, an iodine-based vascular casting resin. Mouse kidneys were imaged *post mortem* with 4 to 5 μm voxel size using a laboratory source absorption-contrast μCT device (GE Nanotom m). Specific obstacles to reliable capillary filling in the kidney were identified, which will aid in development of specialized contrast agents and protocols for *ex vivo* capillary X-ray imaging of the kidney.

2   MATERIALS AND METHODS

2.1   Animal husbandry

C57BL/6J mice were kept in individually ventilated cages with ad libitum access to water and standard rodent food (Kliba Nafag 3436) in 12 h light/dark cycles. All animal experiments were approved by the veterinary office of the canton Zurich (license numbers ZH177/13 and ZH233/15).

2.2   Abdominal aorta perfusion

Mice were anaesthetized with ketamine / xylazine and kidneys were perfused retrogradely via the abdominal aorta based on the isolated perfused kidney technique described by Czogalla et al.[20] Constrictor knot ligations[21] were applied to the abdominal aorta superior of the renal artery and on the superior mesenteric artery to direct all flow to the kidneys. The kidneys were flushed with 10 ml phosphate-buffered saline (PBS) and fixed with 150 mmHg hydrostatic pressure. With the exception of μAngiofil, all contrast agent solutions were injected using a syringe actuated by a constant weight.

2.3   X-ray micro computed tomography

All kidneys were scanned on a Nanotom m X-ray μCT scanner (General Electric, USA) equipped with a water-cooled tungsten target. The X-ray tube was used in mode 0 with an acceleration voltage of 50 kV or 60 kV and a beam current of 310 μA. No additional X-ray filter was applied.

2.4   μAngiofil

Kidneys were flushed with 10 ml PBS and fixed with 100 ml 4% formaldehyde / 0.5% glutaraldehyde in PBS at 150 mmHg hydrostatic pressure. μAngiofil (Fumedica AG, Switzerland) was injected at a constant flow rate of 0.45 ml/min, according to the manufacturer's instructions. Kidneys were excised after polymerization and embedded in 1.5% agar in PBS in a 1.5 ml centrifugation tube. Kidneys were scanned with an acceleration voltage of 50 kV and 4.889 μm voxel size.

2.5   μAngiofil degassed

Kidneys were flushed with 10 ml PBS and fixed with 100 ml 4% formaldehyde / 0.5% glutaraldehyde in PBS at 150 mmHg hydrostatic pressure. μAngiofil was degassed in a vacuum chamber at 90 mbar and injected at a constant flow rate of 0.45 ml/min. Kidneys were excised after polymerization and embedded in 1.5% agar in PBS in a 1.5 ml centrifugation tube. Kidneys were scanned with an acceleration voltage of 50 kV and 4.889 μm voxel size.

2.6   Aurovist 15 nm unfiltered

Kidneys were flushed with 10 ml PBS and fixed with 50 ml 4% formaldehyde at 150 mmHg hydrostatic pressure. Free aldehydes were flushed out with 5 ml PBS and a mixture of 150 μl Aurovist 15 nm (Nanoprobes Inc., USA) with 3% gelatin in 2 ml PBS was injected (15 mg gold/ml). Kidneys were excised, immersed briefly in 4% formaldehyde and embedded in 3% gelatin in PBS in a 1.5 ml centrifugation tube. Kidneys were scanned with an acceleration voltage of 50 kV and 4.444 μm voxel size.

2.7   Aurovist 15 nm filtered

Kidneys were flushed with 10 ml PBS and fixed with 100 ml 2% glutaraldehyde in PBS at 150 mmHg hydrostatic pressure. 200 μl Aurovist 15 nm were mixed with 1.5 ml PBS (23.6 mg gold/ml), pressed through a 1.2 μm pore size

syringe filter and injected into the kidneys. Renal artery and vein of each kidney were ligated immediately afterwards. Kidneys were excised and embedded in 1% agar in PBS in a 0.5 ml PCR tube. Kidneys were scanned with an acceleration voltage of 60 kV and 3.2 µm voxel size.

2.8 ExiTron nano 12000 unfiltered

Kidneys were flushed with 10 ml PBS and fixed with 100 ml 4% formaldehyde / 1% glutaraldehyde in PBS at 150 mmHg hydrostatic pressure. Free aldehydes were flushed out with 15 ml PBS and 0.4 ml ExiTron nano 12000 nanoparticles (nanoPET Pharma GmbH, Germany) in 1.6 ml PBS were injected. Renal artery and vein of each kidney were ligated immediately afterwards. Kidneys were excised and embedded in 6% gelatin with 1% glutaraldehyde in PBS. Kidneys were scanned with an acceleration voltage of 60 kV and 4.4 µm voxel size.

2.9 ExiTron nano 12000 filtered

Kidneys were flushed with 10 ml PBS and fixed with 100 ml 4% formaldehyde / 1% glutaraldehyde in PBS at 150 mmHg hydrostatic pressure. Free aldehydes were flushed out with 20 ml PBS. 0.5 ml ExiTron nano 12000 nanoparticles were mixed with 1.5 ml PBS, filtered through a 0.45 µm pore size syringe filter and injected into the kidneys. Renal artery and vein of each kidney were ligated immediately afterwards. Kidneys were excised and embedded in 1% agar in PBS in a 0.5 ml PCR tube. Kidneys were scanned with an acceleration voltage of 60 kV and 4.444 µm voxel size.

2.10 ExiTron nano 12000 filtered in mannitol

Kidneys were flushed with 10 ml PBS and fixed with 100 ml 4% formaldehyde / 1% glutaraldehyde in PBS at 150 mmHg hydrostatic pressure. 0.5 ml ExiTron nano 12000 nanoparticles were mixed with 1.5 ml isosmotic mannitol solution, filtered through a 1.2 µm pore size syringe filter and injected into the kidneys. Renal artery and vein of each kidney were ligated immediately afterwards. Kidneys were excised and embedded in 1% agar in PBS in a 1.5 ml centrifugation tube. Kidneys were scanned with an acceleration voltage of 60 kV and 4.444 µm voxel size.

2.11 Visualization

Contrast of the virtual sections was manually adjusted for optimal visibility of relevant features of interest using Fiji/ImageJ.[22] Maximum intensity projections were rendered using Bitplane Imaris 8.4.1.
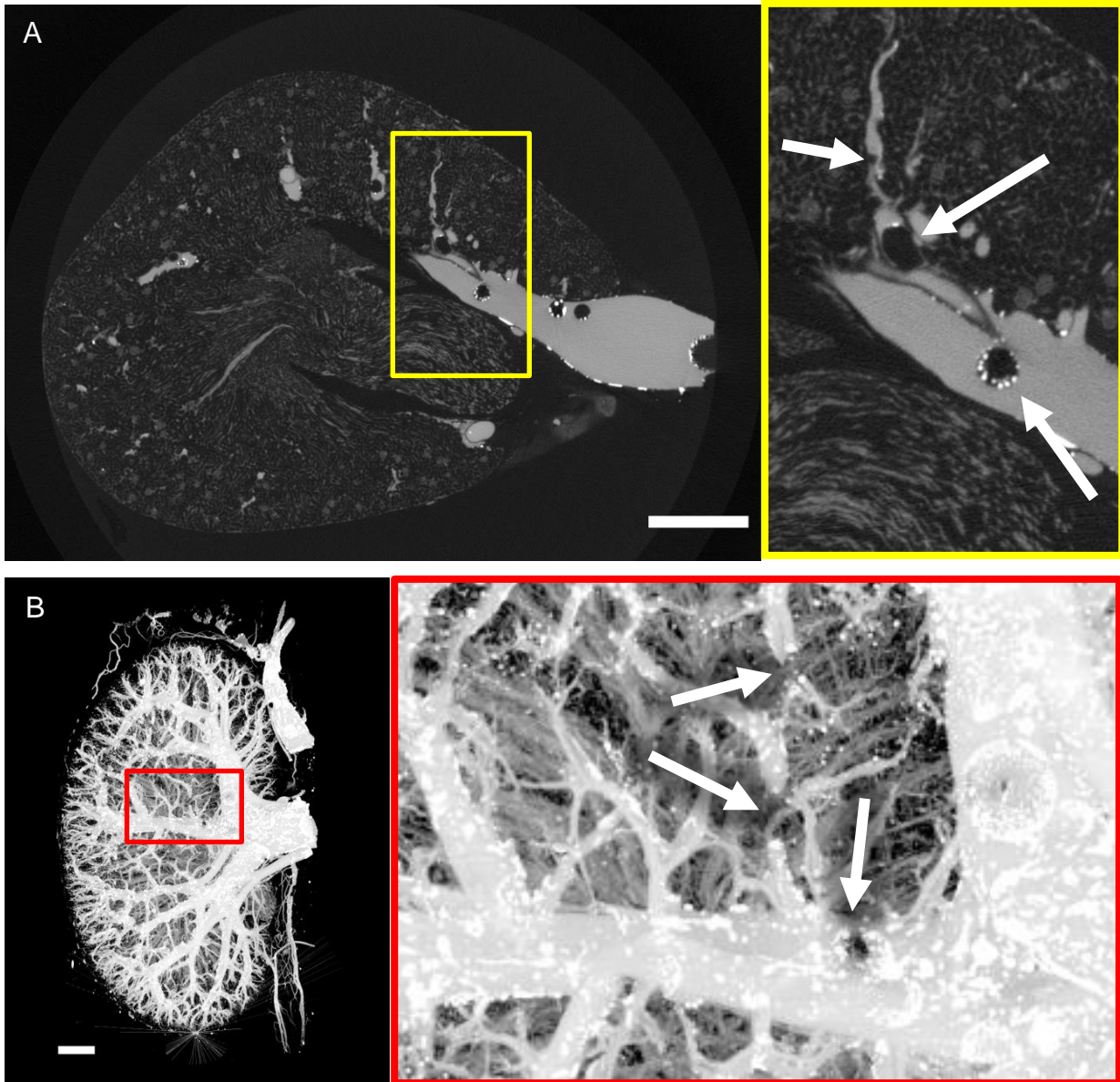
3 RESULTS

3.1 µAngiofil

Figure 1. Virtual section (A) and maximum intensity projection (B) of a mouse kidney perfused with µAngiofil. White arrows indicate gas bubbles in the cast large enough to interrupt the blood vessel. The scale bars correspond to a length of 1 mm.

µAngiofil reached the entire blood vessel system when used according to the manufacturer's instructions. Many gas bubbles, however, formed during polymerization of the contrast agent, best visible in the larger vessels. These bubbles were of sufficient size to interrupt blood vessels (Fig. 1), which would disturb thickness determination and connectivity analysis. Highly X-ray absorbing particles were found primarily at the phase boundaries, likely having formed due to phase separation and accumulation of the radiopaque component of the plastic resin after polymerization.
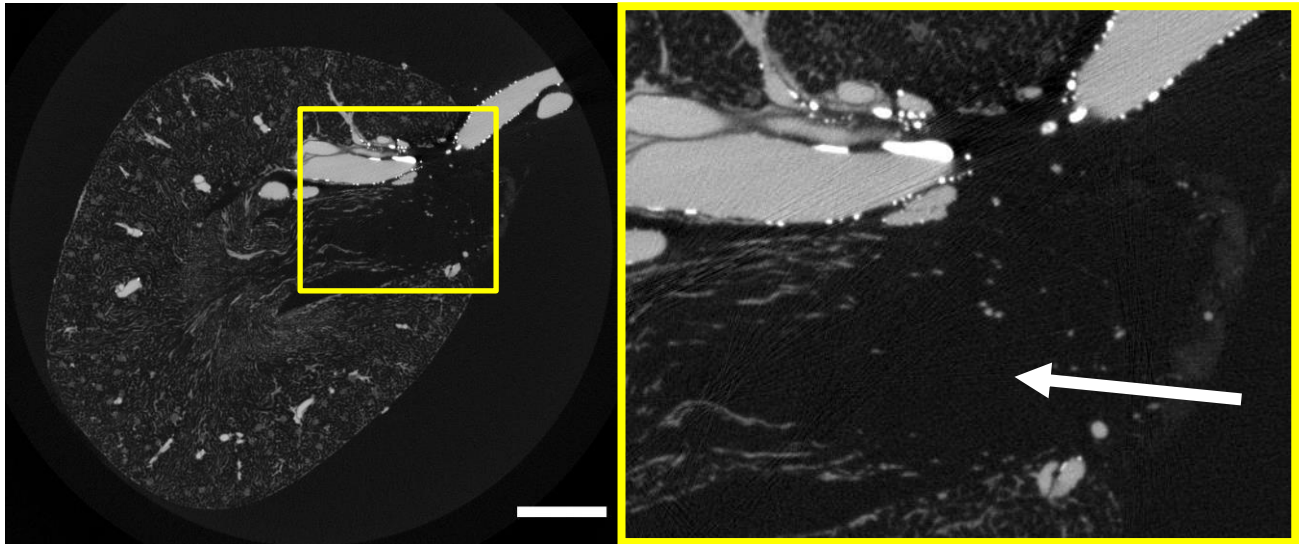
3.2 µAngiofil degassed

Figure 2. Mouse kidney perfused with degassed µAngiofil. The white arrow indicates non-filled vasculature in the inner medulla. The scale bar corresponds to a length of 1 mm.

Degassing of the µAngiofil plastic resin solution in a vacuum chamber prior to perfusion suppressed the formation of gas bubbles (Fig. 2). The vasculature in the inner medulla was no longer completely filled, however, which was likely caused by changes in viscosity of the plastic resin due to evaporation of the solvent during degassing. As the chemical composition of µAngiofil is proprietary information, supplementation of the solvent was not possible for the present study.
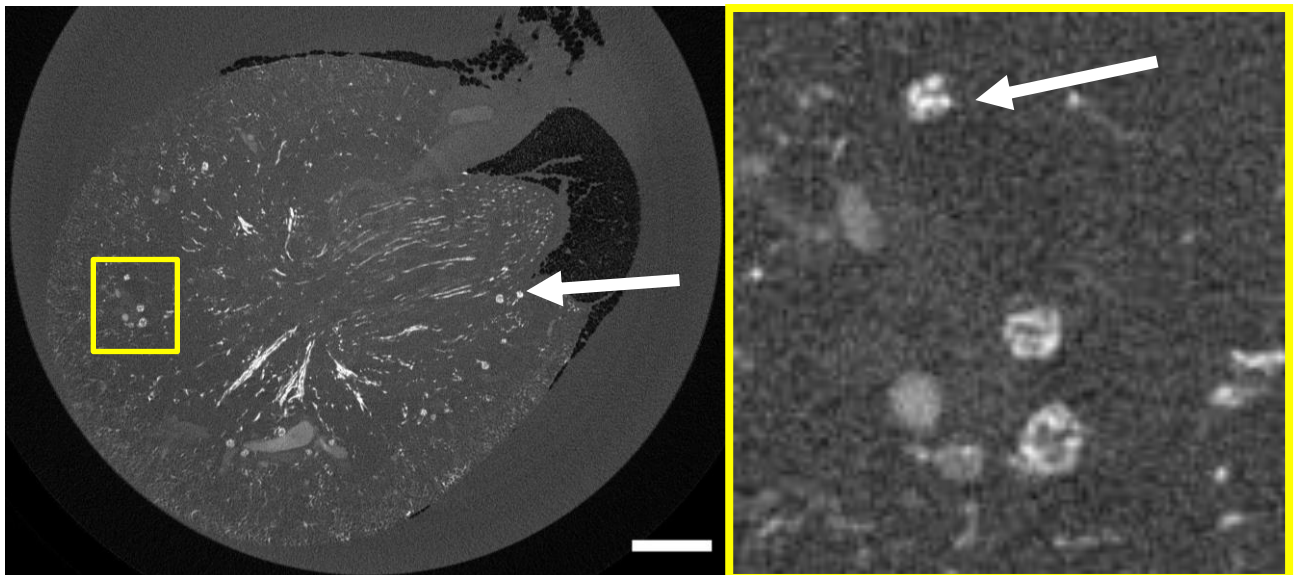
3.3 Aurovist 15 nm unfiltered

Figure 3. Mouse kidney perfused with Aurovist 15 nm. The white arrows indicate glomeruli containing highly absorbing species, suggesting blockage of the capillary loops by aggregated nanoparticles. The scale bar corresponds to a length of 1 mm.

Aurovist 15 nm gold nanoparticles suspended in gelatin did not fill the entire capillary network. Patches of missing vasculature could be found homogeneously distributed throughout the whole kidney volume. Highly absorbing species in the glomeruli suggest that blockage of the capillary loops by aggregated nanoparticles may prevent proper perfusion of the capillary bed. Despite the gelatin perfusion, nanoparticles also slowly diffuse out of the vasculature, reducing contrast over time.
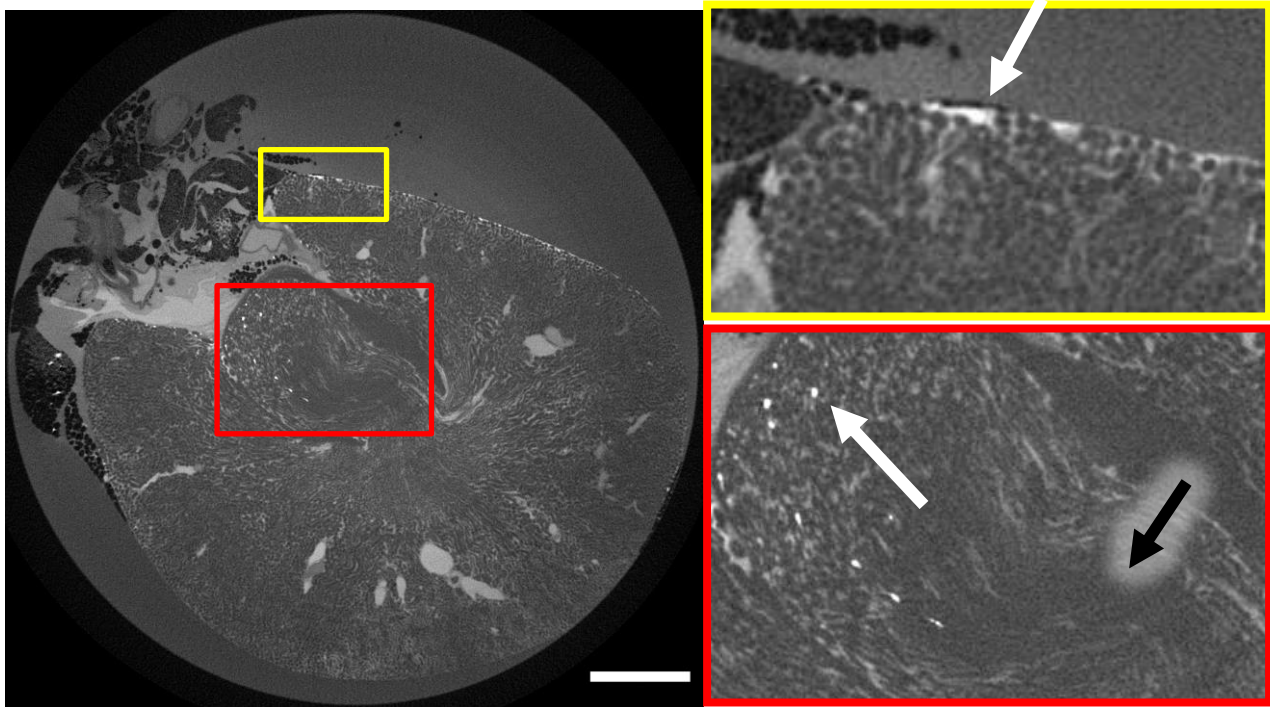
3.4 Aurovist 15 nm filtered

Figure 4. Mouse kidney perfused with filtered Aurovist 15 nm. The black arrow indicates non-filled vasculature in the inner medulla. The white arrows indicate highly absorbing species in the vasa recta and superficial cortical capillaries, suggesting blockage by aggregated nanoparticles. The scale bar corresponds to a length of 1 mm.

Filtered Aurovist 15 nm without gelatin filled almost all of the capillaries in the kidney. A subset of the vasa recta in the inner medulla were not filled, and part of the cortical capillary network showed lower concentrations of contrast agent. Highly absorbing species could be identified in the inner medulla and at the superficial cortical capillaries, suggesting blockage owing to remaining or newly formed aggregates of nanoparticles.
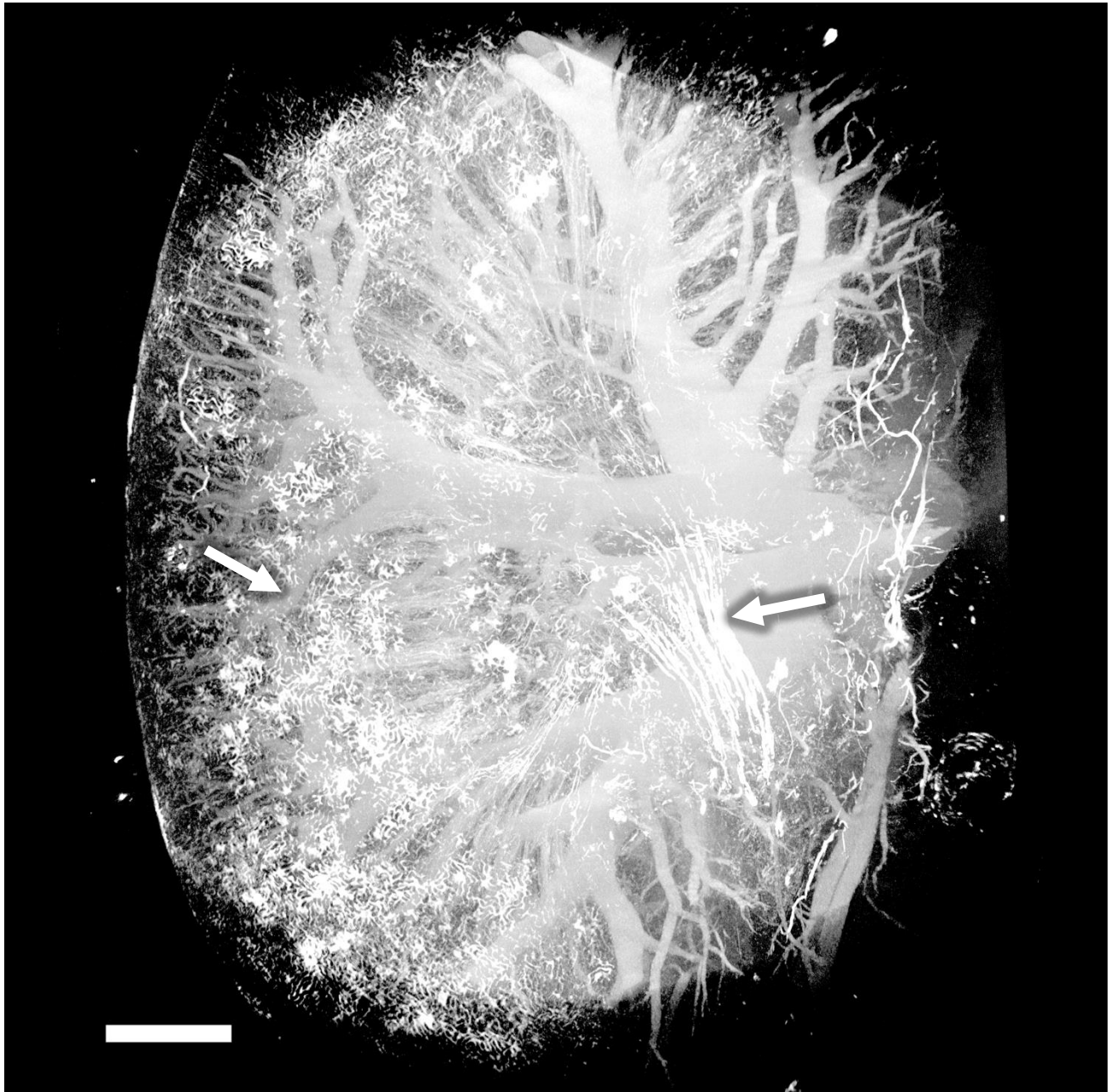
Figure 5. Maximum intensity projection displaying a single height step of a mouse kidney perfused with filtered Aurovist 15 nm. The white arrows indicate highly absorbing species in the vasa recta and superficial cortical capillaries, suggesting blockage by aggregated nanoparticles. The scale bar corresponds to a length of 1 mm.
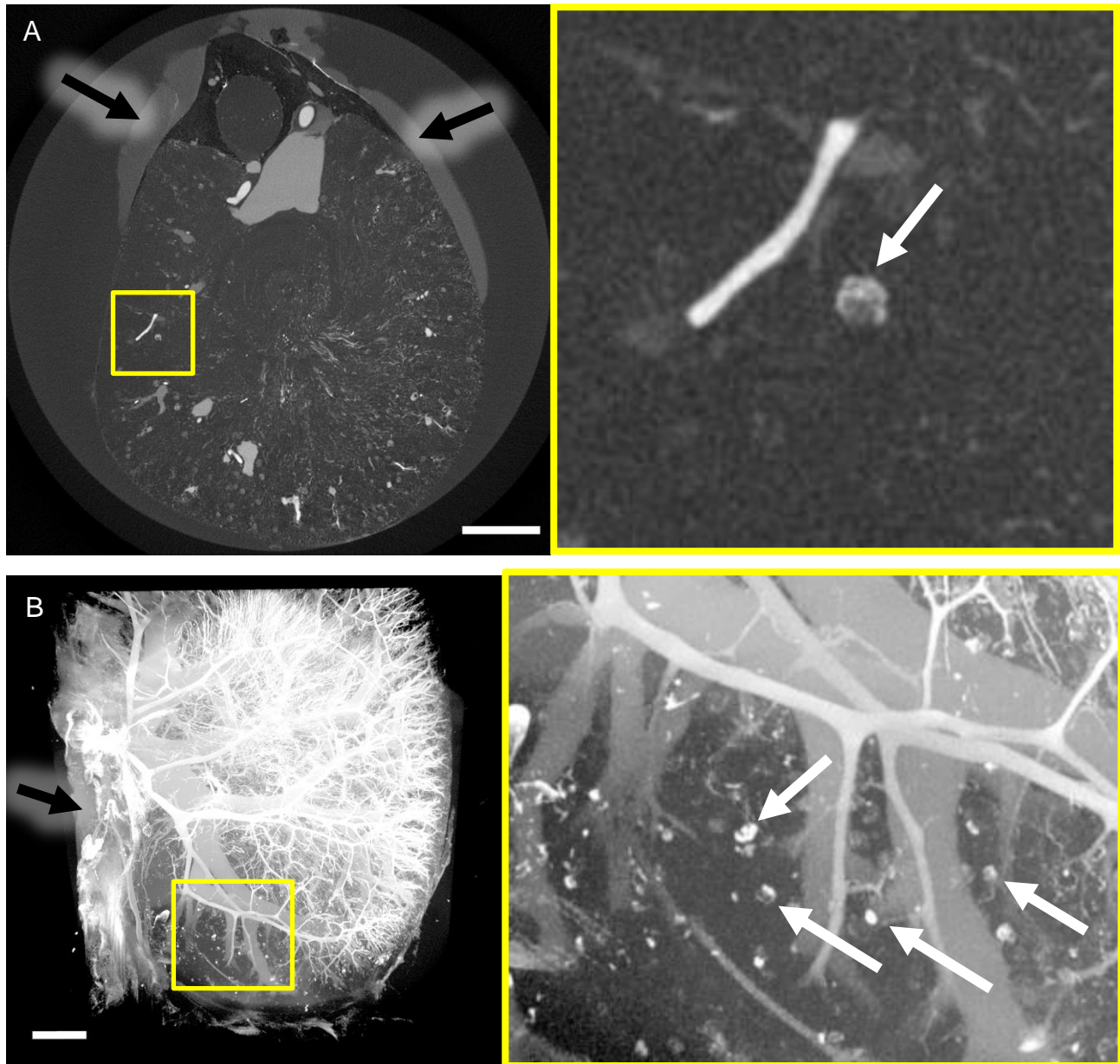
3.5 ExiTron nano 12000 unfiltered

Figure 6. Virtual section (A) and maximum intensity projection (B) of a mouse kidney perfused with unfiltered ExiTron nano 12000. The white arrows indicate glomeruli containing highly X-ray absorbing species, suggesting blockage of the capillary loops by aggregated nanoparticles. The black arrows indicate accumulation of contrast agent leaking into the surrounding agar medium through the renal artery and vein. The scale bars correspond to a length of 1 mm.

Unfiltered ExiTron nano 12000 nanoparticles yielded results similar to unfiltered Aurovist 15 nm nanoparticles. Non-filled capillaries were found in one large cortical region and the associated parts in the medulla. Further small regions with missing vessels were homogeneously distributed throughout the rest of the kidney. Aggregates in the glomeruli suggest that the blockage of the capillary loops prevents further perfusion of the nanoparticles.
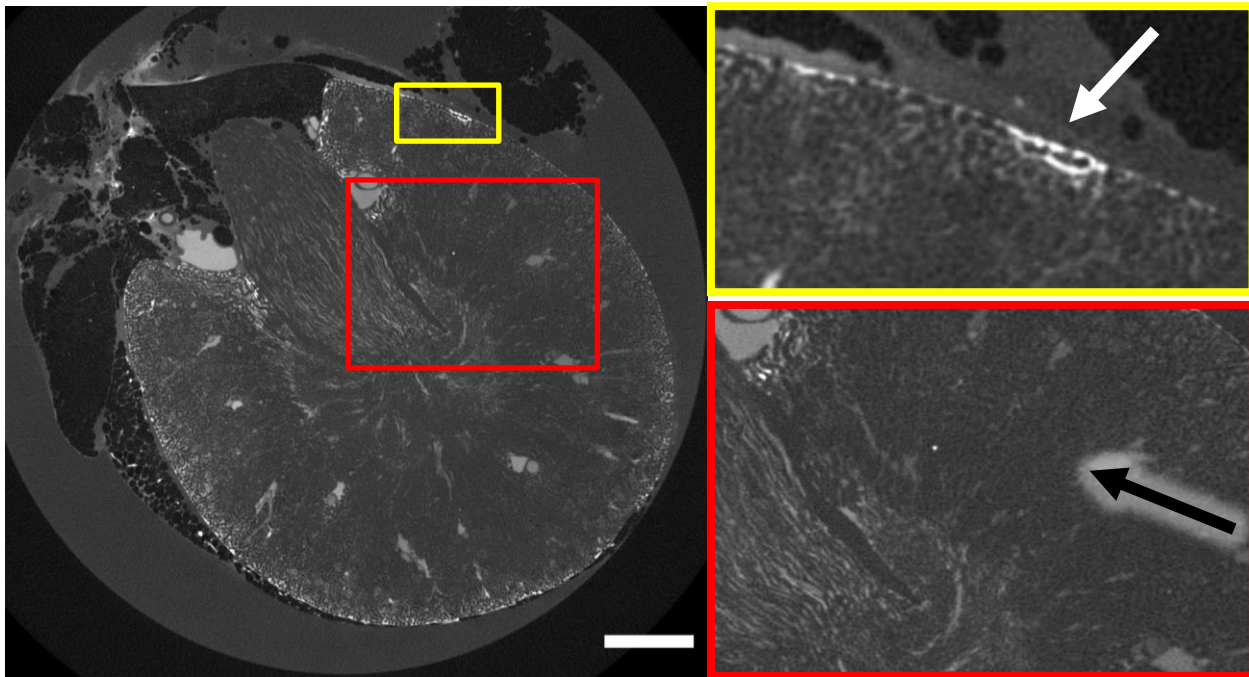
3.6 ExiTron nano 12000 filtered

Figure 7. Mouse kidney perfused with filtered ExiTron nano 12000. The white arrow indicates highly absorbing species in superficial cortical capillaries. The black arrow indicates unfilled vasculature in the cortex and the outer medulla. The scale bar corresponds to a length of 1 mm.

As with Aurovist 15 nm, filtering ExiTron nano 12000 nanoparticles resulted in improved, but still incomplete filling. Empty regions were found in the cortex and the outer medulla. Aggregates could be seen primarily in the superficial capillary network.

3.7 ExiTron nano 12000 filtered in mannitol

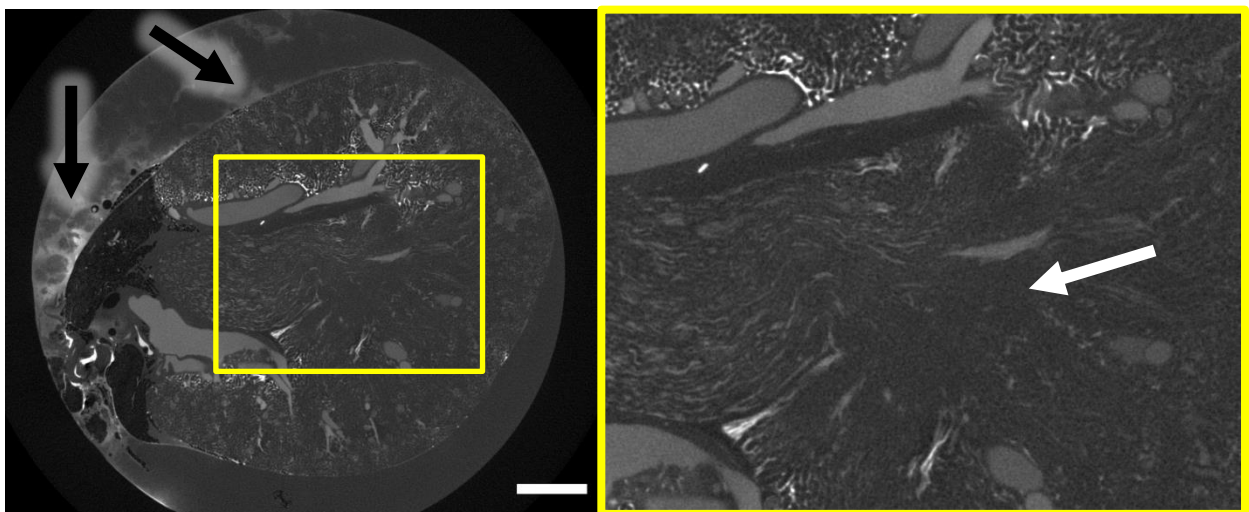Figure 8. Mouse kidney perfused with filtered ExiTron nano 12000, suspended in an isosmotic mannitol solution. The white arrow indicates incompletely filled vasculature in the outer medulla. The black arrows indicate accumulation of contrast agent leaking into the surrounding agar medium through superficial capillaries or the renal artery and vein. The scale bar corresponds to a length of 1 mm.

Based on suggestions from the manufacturer, ExiTron nano 12000 nanoparticles were suspended in isosmotic mannitol solution instead of PBS to reduce aggregation of the particles. Regions with incompletely filled capillaries could still be found. Aggregated nanoparticles were still present, albeit in capillaries in the vicinity of large vessels, rather than superficial capillaries.
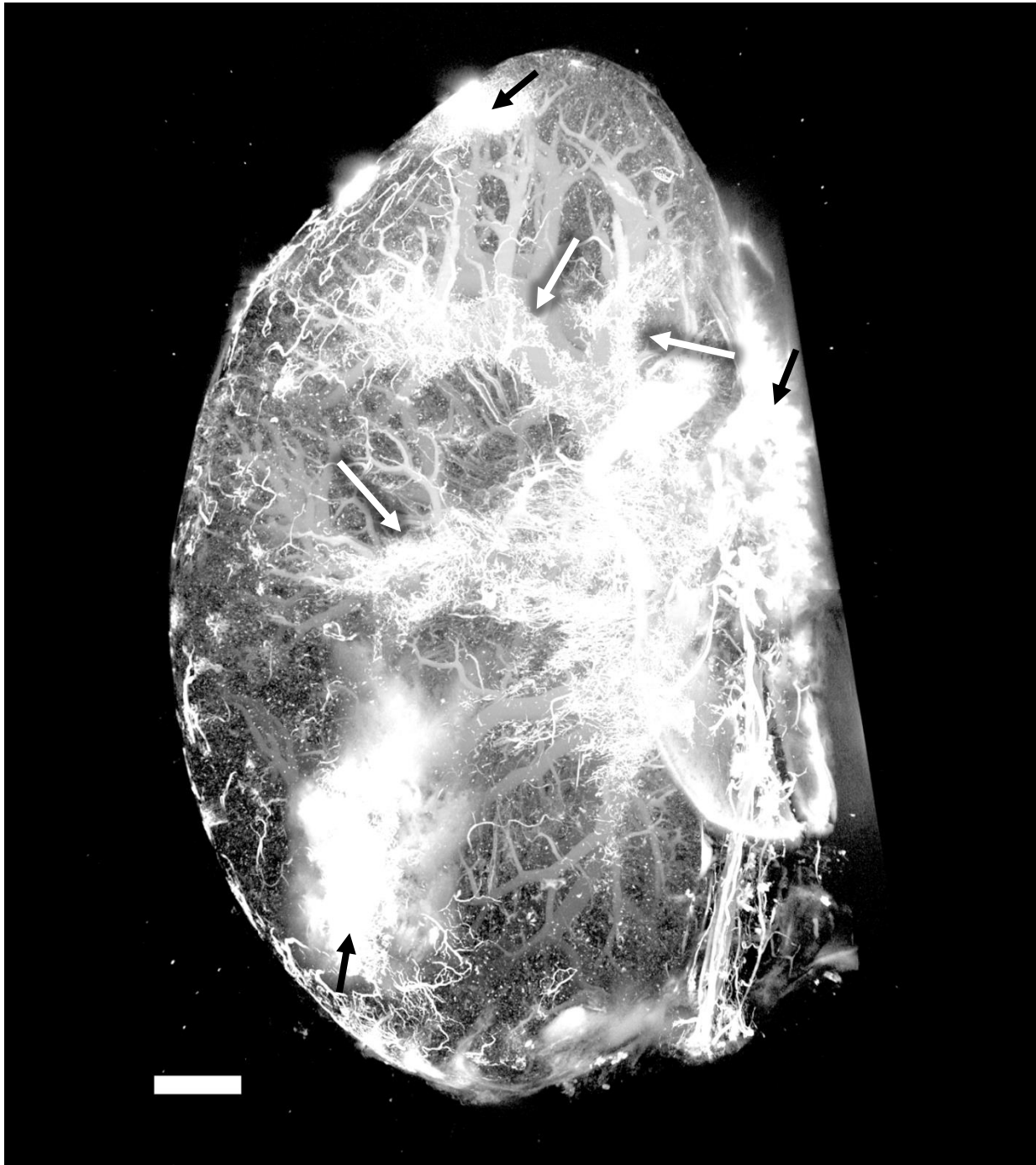
Figure 9. Maximum intensity projection of a mouse kidney perfused with filtered ExiTron nano 12000, suspended in an isosmotic mannitol solution. The white arrows indicate capillaries filled with aggregates surrounding large blood vessels. The black arrows indicate accumulation of contrast agent leaking into the surrounding agar medium through superficial capillaries or the renal artery and vein. The scale bar corresponds to a length of 1 mm.

4   DISCUSSIONS

In preclinical studies investigating capillary rarefaction, it is crucial that vascular imaging data is reliable, complete and representative of the vasculature in order to prevent false-negatives. In this study, contrast agents were evaluated solely based on their ability to fill the entire renal vasculature. Contrast-to-noise is influenced by factors independent of the choice of contrast agent, such as the type and quality of µCT equipment. Contrast agents feature different heavy elements as radiopaque component, were used in different concentrations and scanned at comparable but slightly different photon energies. Intensity values and contrast-to-noise therefore should not be compared across contrast agents based on the data presented in this study, and structures could not be segmented on an equivalent basis. In addition, there is no single objective measure capable of encompassing the widely differing types of filling artifacts. Quantitative measures such as vessel density and non-perfused area would not accurately reflect issues with vessel discontinuities. Conversely, connectivity analysis would not accurately reflect non-perfused kidney regions, when the perfused regions show no discontinuities within themselves. Comparisons of different protocols would therefore only be possible based on subjective weighting of multiple factors, even if segmentation on equal grounds had been achieved. Contrast agent filling was thus evaluated only on a qualitative basis.

The vascular casting resin µAngiofil was capable of filling all capillaries, but produced a large amount of gas bubbles during polymerization, leading to disconnected vessel segments. Since µAngiofil is a hydrophobic plastic resin, particular care has to be taken to ensure thorough flushing of the kidney vasculature from any remaining water, which could otherwise lead to water inclusions, which are another source of vessel discontinuities. Plastic resins also feature higher viscosities than water-soluble X-ray contrast agents. Flow rates have to be optimized and adjusted individually when perfusing kidneys with capillary rarefaction, as these feature a lower blood flow capacity. Otherwise, high pressures during perfusion may lead to bursting vessels, distension of blood vessels and collapse of tubular lumina.

Aurovist 15 nm and ExiTron nano 12000 are both surface-functionalized metal nanoparticles, and their results were comparable to each other, despite their different particle sizes of 15 nm and 110 nm, respectively. Unfiltered nanoparticles were unable to fill the whole capillary bed of the kidneys. Highly X-ray absorbing species visible in the glomeruli suggest that nanoparticle aggregates block the glomerular capillary loops, which are located at the beginning of the capillary network. Blockage at this location would result in the observed lack of perfusion in various kidney regions, as these are downstream of the glomeruli.

Filtering the nanoparticles with syringe filters greatly reduced the number of aggregates, but was unable to remove them completely. Accordingly, unfilled capillaries remained, although at much lower numbers. The aggregates were considerably larger than the pore size of the filters, which suggests that they were formed after filtration within the kidney. To reduce aggregation, ExiTron nano 12000 was suspended in isosmotic mannitol solution instead of PBS in accordance to suggestions from the manufacturer. However, capillary filling did not improve. While aggregation behavior was successfully altered, it only resulted in a shift in location of the aggregates from the kidney surface to the capillaries close to the large blood vessels. Nanoparticles also diffused out of the kidney over time, resulting in loss of signal and increase of background over time, requiring X-ray scans to be performed immediately after sample preparation.

Co-injecting Aurovist 15 nm with gelatin did not prevent diffusion of the nanoparticles out of the vasculature. Capillary filling was negatively affected. Since gelatin solidifies based on temperature, accurate control of this process is challenging and premature solidification can cause incompletely perfused vessels. Gelatin perfusions are therefore not recommended.

Based on these results, the following requirements were identified for a contrast agent to be used in kidney capillary imaging:

1. The contrast agent should be highly water-soluble to prevent issues with discontinuous vessel segments caused by water inclusions of hydrophobic resins and issues of aggregation of suspended particles.

2. The contrast agent needs to be large enough to avoid extravasation or glomerular filtration.

3. The contrast agent should be cross-linkable to prevent loss of contrast and increase of background over time.

A highly water-soluble blood pool contrast agents exists in the form of ExiTron P, a polymeric iodine-based contrast agent. However, this contrast agent has a molecular weight of around 20 000 g/mol and is thus too small to avoid glomerular filtration. As such, while nanoparticle-based blood pool contrast agents represent a substantial advancement over microparticle-based protocols[23,24], there is currently no ideal X-ray contrast agent for *ex vivo* capillary imaging of the kidney available, creating a demand for the development of compounds that fulfill the requirements summarized above. The benefits of such a development would not be limited to studies of the mouse kidney, but also extend to studies of other tissue featuring permeable vasculature, such as tumors[25] or the circumventricular organs in the brain[26].

5 ACKNOWLEDGEMENTS

6 REFERENCES

[1] Saran, R., Robinson, B., Abbott, K. C., Agodoa, L. Y. C., Bragg-Gresham, J., Balkrishnan, R., Bhave, N., Dietrich, X., Ding, Z., Eggers, P. W., Gaipov, A., Gillen, D., Gipson, D., Gu, H., Guro, P., Haggerty, D., Han, Y., He, K., Herman, W., et al., "US Renal Data System 2018 Annual Data Report: Epidemiology of Kidney Disease in the United States," American Journal of Kidney Diseases **73**(3), A7–A8 (2019).

[2] Kida, Y., Tchao, B. N. and Yamaguchi, I., "Peritubular capillary rarefaction: a new therapeutic target in chronic kidney disease," Pediatr. Nephrol. **29**(3), 333–342 (2014).

[3] Mayer, G., "Capillary rarefaction, hypoxia, VEGF and angiogenesis in chronic renal disease," Nephrology Dialysis Transplantation **26**(4), 1132–1137 (2011).

[4] Ehling, J., Bábíčková, J., Gremse, F., Klinkhammer, B. M., Baetke, S., Knuechel, R., Kiessling, F., Floege, J., Lammers, T. and Boor, P., "Quantitative Micro-Computed Tomography Imaging of Vascular Dysfunction in Progressive Kidney Diseases," J. Am. Soc. Nephrol. **27**(2), 520–532 (2016).

[5] Hlushchuk, R., Zubler, C., Barre, S., Correa Shokiche, C., Schaad, L., Rothlisberger, R., Wnuk, M., Daniel, C., Khoma, O., Tschanz, S. A., Reyes, M. and Djonov, V., "Cutting-edge microangio-CT: new dimensions in vascular imaging and kidney morphometry," Am J Physiol Renal Physiol **314**(3), F493–F499 (2018).

[6] Tuna, I. S. and Tatli, S., "Contrast-enhanced CT and MR imaging of renal vessels," Abdom Imaging **39**(4), 875–891 (2014).

[7] Hull, T. D., Agarwal, A. and Hoyt, K., "New Ultrasound Techniques Promise Further Advances in AKI and CKD," JASN **28**(12), 3452–3460 (2017).

[8] Ogunlade, O., Connell, J. J., Huang, J. L., Zhang, E., Lythgoe, M. F., Long, D. A. and Beard, P., "In vivo three-dimensional photoacoustic imaging of the renal vasculature in preclinical rodent models," American Journal of Physiology-Renal Physiology **314**(6), F1145–F1153 (2018).

[9] Hall, A. M., Schuh, C. D. and Haenni, D., "New frontiers in intravital microscopy of the kidney:," Current Opinion in Nephrology and Hypertension **26**(3), 172–178 (2017).

[10] Sandoval, R. M. and Molitoris, B. A., "Intravital multiphoton microscopy as a tool for studying renal physiology and pathophysiology," Methods **128**, 20–32 (2017).

[11] Busse, M., Müller, M., Kimm, M. A., Ferstl, S., Allner, S., Achterhold, K., Herzen, J. and Pfeiffer, F., "Three-dimensional virtual histology enabled through cytoplasm-specific X-ray stain for microscopic and nanoscopic computed tomography," Proc Natl Acad Sci USA **115**(10), 2293–2298 (2018).

[12] Missbach-Guentner, J., Pinkert-Leetsch, D., Dullin, C., Ufartes, R., Hornung, D., Tampe, B., Zeisberg, M. and Alves, F., "3D virtual histology of murine kidneys – high resolution visualization of pathological alterations by micro computed tomography," Sci Rep **8**(1), 1407 (2018).

[13] Shirai, R., Kunii, T., Yoneyama, A., Ooizumi, T., Maruyama, H., Lwin, T.-T., Hyodo, K. and Takeda, T., "Enhanced renal image contrast by ethanol fixation in phase-contrast X-ray computed tomography," J Synchrotron Rad **21**(4), 795–800 (2014).

[14] Pappenheimer, J. R., Renkin, E. M. and Borrero, L. M., "Filtration, diffusion and molecular sieving through peripheral capillary membranes; a contribution to the pore theory of capillary permeability," Am. J. Physiol. **167**(1), 13–46 (1951).

[15] Lusic, H. and Grinstaff, M. W., "X-ray-Computed Tomography Contrast Agents," Chem. Rev. **113**(3), 1641–1666 (2013).

[16] Nebuloni, L., Kuhn, G. A. and Muller, R., "A comparative analysis of water-soluble and blood-pool contrast agents for in vivo vascular imaging with micro-CT," Acad Radiol **20**(10), 1247–1255 (2013).

[17] Hainfeld, J. F., Smilowitz, H. M., O'Connor, M. J., Dilmanian, F. A. and Slatkin, D. N., "Gold nanoparticle imaging and radiotherapy of brain tumors in mice," Nanomedicine **8**(10), 1601–1609 (2013).

[18] Boll, H., Figueiredo, G., Fiebig, T., Nittka, S., Doyon, F., Kerl, H. U., Nölte, I., Förster, A., Kramer, M. and Brockmann, M. A., "Comparison of Fenestra LC, ExiTron nano 6000, and ExiTron nano 12000 for Micro-CT Imaging of Liver and Spleen in Mice," Academic Radiology **20**(9), 1137–1143 (2013).

[19] Detombe, S. A., Dunmore-Buyze, J. and Drangova, M., "Evaluation of eXIA 160XL cardiac-related enhancement in C57BL/6 and BALB/c mice using micro-CT: EVALUATION OF EXIA 160XL CARDIAC ENHANCEMENT," Contrast Media Mol. Imaging **7**(2), 240–246 (2012).

[20] Czogalla, J., Schweda, F. and Loffing, J., "The Mouse Isolated Perfused Kidney Technique," Journal of Visualized Experiments **117**, 54712 (2016).

[21] Hazenfield, K. M. and Smeak, D. D., "In vitro holding security of six friction knots used as a first throw in the creation of a vascular ligation," J Am Vet Med Assoc **245**(5), 571–577 (2014).

[22] Schindelin, J., Arganda-Carreras, I., Frise, E., Kaynig, V., Longair, M., Pietzsch, T., Preibisch, S., Rueden, C., Saalfeld, S., Schmid, B., Tinevez, J. Y., White, D. J., Hartenstein, V., Eliceiri, K., Tomancak, P. and Cardona, A., "Fiji: an open-source platform for biological-image analysis," Nat Methods **9**(7), 676–682 (2012).

[23] Plouraboue, F., Cloetens, P., Fonta, C., Steyer, A., Lauwers, F. and Marc-Vergnes, J.-P., "X-ray high-resolution vascular network imaging," J Microsc **215**(2), 139–148 (2004).

[24] Müller, B., Fischer, J., Dietz, U., Thurner, P. J. and Beckmann, F., "Blood vessel staining in the myocardium for 3D visualization down to the smallest capillaries," Nuclear Instruments and Methods in Physics Research Section B: Beam Interactions with Materials and Atoms **246**(1), 254–261 (2006).

[25] Lang, S., Müller, B., Dominietto, M. D., Cattin, P. C., Zanette, I., Weitkamp, T. and Hieber, S. E., "Three-dimensional quantification of capillary networks in healthy and cancerous tissues of two mice," Microvascular Research **84**(3), 314–322 (2012).

[26] Ganong, W. F., "Circumventricular organs: definition and role in the regulation of endocrine and autonomic function," Clin. Exp. Pharmacol. Physiol. **27**(5–6), 422–427 (2000).